Kinematics of steep bedrock permafrost

Andreas Hasler,[1] Stephan Gruber,[1] and Jan Beutel[2]

Received 11 February 2011; revised 9 December 2011; accepted 14 December 2011; published 22 February 2012.

[1] The mechanisms that control climate-dependent rockfall from permafrost mountain slopes are currently poorly understood. In this study, we present the results of an extensive rock slope monitoring campaign at the Matterhorn (Switzerland) with a wireless sensor network. A negative dependency of cleft expansion relative to temperature was observed at all clefts for the dominant part of the year. At many clefts this process is interrupted by a period with increased opening and shearing activity in the summer months. More specific, this period lasts from sustained melting within the cleft to the first freezing in autumn. Based on these empirical findings we identify two distinct process regimes governing the cleft motion observed. Combining current theories with laboratory evidence on rock slope movement and stability, we postulate that (1) the negative temperature-dependency is caused by thermomechanical forcing and is reinforced by cryogenic processes during the freezing period and, (2) the enhanced movement in summer originates from a hydro-thermally induced strength reduction in clefts containing perennial ice. It can be assumed that the irreversible part of the process described in (1) slowly modifies the geometric settings and cleft characteristics of permafrost rock slopes in the long term. The thawing related processes (2) can affect stability within hours or weeks. Such short-term stability minima may activate rock masses subject to the slow changes and lead to acceleration and failure.

Citation: Hasler, A., S. Gruber, and J. Beutel (2012), Kinematics of steep bedrock permafrost, *J. Geophys. Res.*, *117*, F01016, doi:10.1029/2011JF001981.

1. Introduction and Problem Statement

[2] Steep bedrock in high-alpine regions such as the European Alps is influenced by seasonal frost or permafrost. Permafrost degradation and changes in the thermal and hydrological regime in these areas as a result of changing climatic conditions can directly affect man-made infrastructure, cause increased rockfall activity, or trigger natural disasters via process chains [*Haeberli et al.*, 1997]. The hypothesis that such climate related processes are relevant to alpine geomorphodynamics and rock destabilization is supported by (1) the exceptional rockfall that occurred in the hot summer of 2003 in the European Alps [*Gruber et al.*, 2004], (2) the correlation of regional rockfall activity with warm decades in the past century [*Fischer*, 2010; *Ravanel and Deline*, 2010], and (3) the presence of ice at the failure surface of high-alpine rockfalls as reported by *Gruber and Haeberli* [2007], *Pirulli* [2009], and *Fischer et al.* [2010]. The processes linking climate change and rockfall in high-alpine regions and the role of permafrost in rockfall release are currently poorly understood but several studies focus on physical processes and phenomena that are closely related. These studies state that ice formation processes are an efficient contribution to rock weathering and fracture widening [*Hallet et al.*, 1991; *Matsuoka*, 2001a; *Coussy*, 2005; *Murton et al.*, 2006] and that the pore ice content influences the geotechnical properties of intact rock [*Mellor*, 1973]. Furthermore, changes in ice temperature and geometries affect the mechanical properties of the rock discontinuity [*Davies et al.*, 2001; *Guenzel*, 2008] and so permafrost degradation can modify the hydraulic permeability leading to a possible build-up in hydrostatic pressure within previously ice-sealed fractured rock and its downslope hydrological regime [*Haeberli et al.*, 1997]. *Fischer* [2010] discussed different factors that contribute to the stability of high alpine slopes and arranged them in a continuum between disposing factors and trigger factors. Accordingly, lithology, structure and topography of rock slopes are dominating factors for the disposition to rockfall but they remain rather constant within the timescales considered in the discussion of climate change impact (decades to millennia). Further, rock fatigue and subcritical fracture propagation [*Atkinson*, 1982; *Kemeny*, 2003] can lead to rock weakening and failure without the presence of an obvious trigger. In contrast, glaciers, ice faces, permafrost and hydrothermal conditions within rock faces are directly influenced by climate change and subject to the corresponding response times. Therefore, these phenomena and their influence on rock stability are essential for the understanding of recent and future development of hazards originating from high-alpine bedrock.

[1]Glaciology, Geomorphodynamics and Geochronology, Department of Geography, University of Zurich, Zurich, Switzerland.
[2]Computer Engineering and Networks Laboratory, ETH Zurich, Zurich, Switzerland.

0148-0227/12/2011JF001981

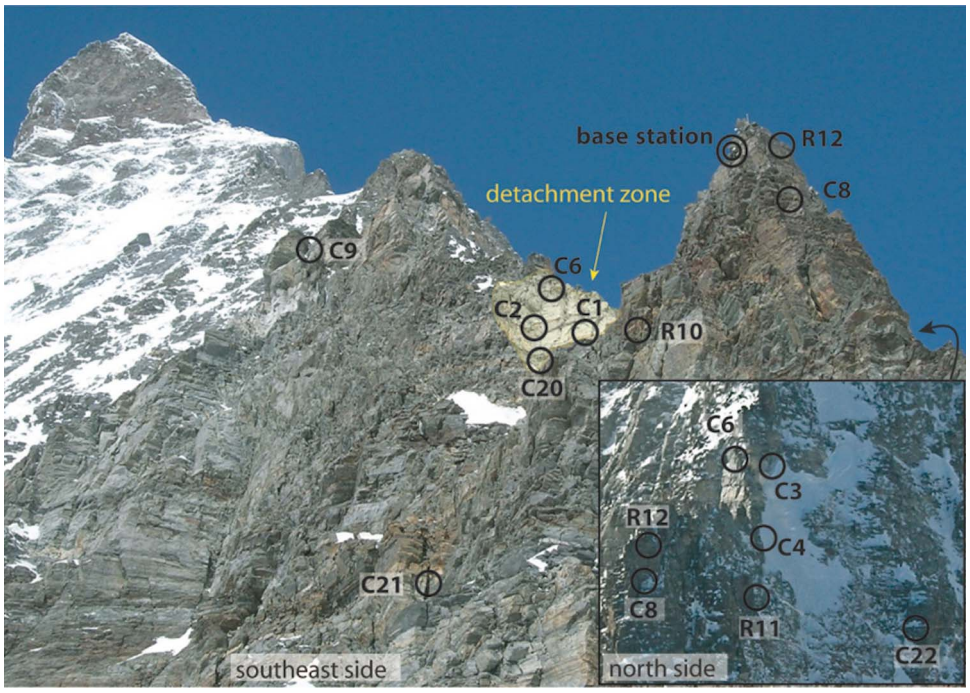

Figure 1. Overview of the Matterhorn Hörnligrat site from southeast and northeast (inset). The circles with labels indicate the sensor locations. C stands for cleft (expansion and temperatures) and R stands for shallow rock boreholes (temperatures and electrical resistance).

[3] In this study we focus on steep high-alpine rock faces that were not subject to recent glacier or ice retreat. We aim to identify the processes of thermal and hydrologic control on deformation and related rockfall. Rock movements are not necessarily only pre-failure deformations but may be part of slow moving instabilities (rock creep) or reversible (quasi-elastic) movements. The investigation of the mode and evolution of these slow movements allows us to infer the driving forces and processes of an event [*Braathen et al.*, 2004]. In this study we have analyzed the seasonal evolution of deformation with high temporal resolution considering spatial movement modes such as toppling, buckling and sliding [*Cruden*, 2003] qualitatively where clear geomorphic evidence exists. For this purpose, an analysis of the relative deformation (dilatation and shear) in rock clefts and the temperatures in the active layer of permafrost rock faces at Matterhorn Hörnligrat (Swiss Alps) has been performed. We use the term cleft for open rock fractures that experience opening (joints) or shearing (shear-fractures; faults). Most deformation in hard brittle rock occurs along these (pre-existing) discontinuities and causes relative movements of the blocks of rock [*Eberhardt et al.*, 2004]. At high-alpine sites with differing mechanical and lithological settings similar movements with cleft expansion in autumn and contraction in spring have been observed [*Matsuoka*, 2001a, 2008; *Nordvik et al.*, 2010; *Wegmann and Gudmundsson*, 1999]. Because of these apparent similarities we expect common mechanisms which are not masked by geological circumstances.

[4] In the first part of this paper we describe the situation, measurement setup and results derived from two and a half years of recordings of temperatures and cleft movements in the active layer of steep bedrock permafrost (Section 2–4). We then elaborate on typical patterns observed and correlations found within these data, and develop hypotheses about the driving mechanisms behind the empirical findings (Section 5). This hypothesis-generating approach follows that of *Matsuoka* [2001a, 2008] but differs regarding the cleft dimensions and rock masses considered.

2. Site Description

2.1. Topographic and Climatic Situation

[5] The summit of Matterhorn, 4478 m high, is part of the main divide of the western Alps that marks the Swiss-Italian border. The northeastern ridge also known as the Hörnligrat is one of the most famous ascents in the Alps attracting more than a thousand alpinists per year. In July 2003 a rockfall occurred at the base of the ridge near the top of the so-called second couloir and 84 climbers had to be evacuated (B. Jelk, personal communication, 2009). The ice-filled clefts observed immediately after the detachment of this rockfall, the strong fracturing, the large gradient of surface thermal conditions and the suspected deformation in proximity of the detachment zone motivated the selection of this site. In October 2007 a first installation of temperature sensors and geo-technical instruments was performed within and near the detachment zone [*Hasler et al.*, 2008]. An extension of this initial deployment was undertaken in June 2010 involving a cluster of 17 measurement devices distributed across the site (Figure 1).

[6] The field site is located at an elevation of 3500 m a.s.l. and comprises both sides of the ridge with main orientations south-southeast and north-northwest at the given elevation

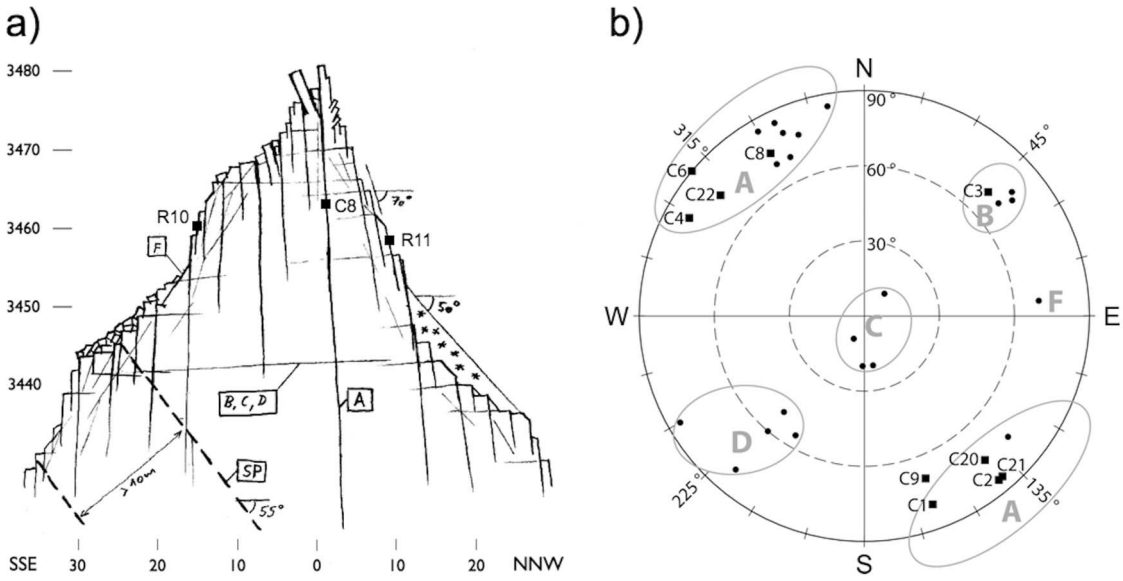

Figure 2. Geometry and structural situation of the installation site (3440–3480 m a.s.l.) at the Matterhorn Hörnligrat. (a) Profile sketch through the ridge (A–F, cleft families; SP, faults beneath the installation site; left scale, elevation; bottom scale, distance from ridge (m)). (b) Polar plot (upper hemisphere) of the cleft orientation (normal) of 21 sampled clefts (dots) and the clefts instrumented with crack meters (squares and sensor labels) with corresponding cleft families (A–F).

(Figure 1). The northern side contains small ice fields within a steep heterogeneous rock face, which is dominantly snow-free accumulating a thin snow cover only sporadically in winter. On the south side, snow patches develop during winter in couloirs and on rock bands, which are partly debris covered (Figure 2). These snow patches on the south side disappear in spring/summer completely. The bottom of both rock faces is glaciated, on the southeastern side leading into a plateau formed by the Furgg glacier. The mean annual air temperature (MAAT, average 1961–1990) is −6.7°C [*Hiebl et al.*, 2009] and the typical annual precipitation is assumed to be greater than 1000 mm/a although accurate estimates are difficult to obtain due to the proximity to the meteorological divide and a large elevation difference to the next meteorological station (Zermatt) operated by the Swiss Meteorological Service. Except for some occasional summer rainfalls the dominant precipitation falls as snow hence liquid water is mainly supplied to the site by snowmelt.

2.2. Geology and Structure

[7] Geologically, the main part of the Matterhorn summit consists of gneiss and amphibolite of the Dent Blanch nappe [*Pleuger et al.*, 2007]. The site is 30–100 m above the interface with the underlying Tsaté series of the Combin zone (mainly Bündnerschiefer and ophiolite) [*Pleuger et al.*, 2007]. The lower part of the Hörnligrat (<3800 m a.s.l.) is strongly fractured but the rock in the northern face shows many lichens, indicating a rather low erosive activity. Typically, cleft spacing is 0.2–2 m with apertures of 3–30 cm. The most dominant cleft family (see location of family A in Figure 2) is oriented parallel to the ridge and dips nearly vertical. These clefts have an extent of 3–40 m. Several signs of toppling movements lateral to the ridge are visible. This tilting of (free standing) rock pillars and flakes differs from slope toppling situations because the shearing movement at the contact with the neighboring blocks only dominates in the root zone of the blocks (compare, e.g., *Savage and Varnes* [1987]. Further up the ridge close to location 9 (Figure 1), these near-vertical clefts cluster into two separate families, one dipping at 75° southeast and the other dipping at 75° northwest. A second cleft family is visible near-horizontal corresponding with the schistosity of the amphibolite (see location of family C in Figure 2). The cleft families B and D are inclined with respect to family C but also perpendicular to the ridge (overlap with family C in Figure 2a). The mineral orientation of the gneiss builds the weakness planes for these clefts. The extent of the clefts and free surfaces of these families is 0.1–2 m. Often their extent is limited by the clefts of family A. Faults with more than ten meters spacing dip 55° northwesterly. Their shearing direction could not be assessed because the offset of the bedding is not obvious. In addition to the cleft families described there are inferior surface-parallel clefts and free surfaces visible although they could not be assigned to a particular family. The only surface with such an orientation and a significant persistence in proximity of the rockfall zone is the detachment surface itself (see location of family F in Figures 2 and 3).

2.3. Rockfall of Summer 2003

[8] The Matterhorn rockfall of 2003 had a decisive influence on the field site therefore a brief description of this event is provided. The summer 2003 in Switzerland was approximately 3°C warmer than the long-term average and was characterized by a long period with very little precipitation [*Gruber et al.*, 2004]. A total volume of 1000–2000 m^3 of rock detached in two distinct events on 15 and 16 July respectively. The early timing within the year (little advanced thawing front) and no obvious triggering such as heavy precipitation was characteristic for the exceptional rockfalls in this summer [*Gruber et al.*, 2004]. The rock mass detached at

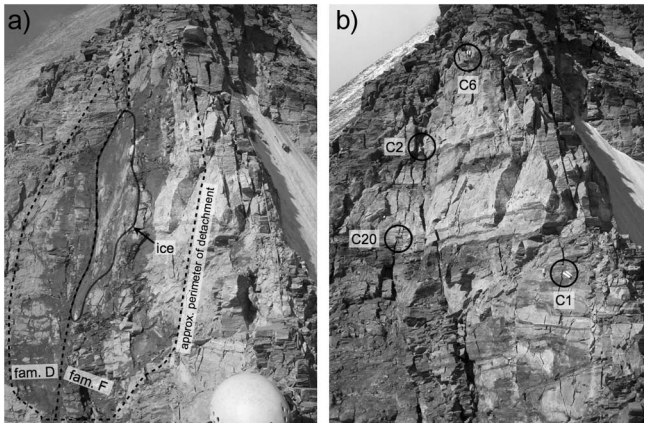

Figure 3. Close-up of the detachment zone of the rockfall in summer 2003. (a) Detachment zone some hours after the 2nd rockfall on 16 July 2003 (photography by B. Jelk). (b) Detachment zone with sensor locations in August 2010. The failure surface consists of different surfaces of the family F where ice was visible after the event in 2003 and a cleft of the family B.

the southern side of the ridge above a small saddle (Figure 1). The base of the detached rock mass is located at the top of a couloir and does not show a sliding plane. Lateral detachment surfaces correspond to a cleft of the family B and the main failure plane F (Figure 2). The first event (15 July) comprised the lower right hand part of the rock mass whereas a pillar remained in the corner between B and F until it collapsed less than a day later. At the failure plane ice was observed shortly after the second event took place (Figure 3).

3. Measurement Setup

3.1. Instrumentation

[9] Acquiring distributed long-term measurements in harsh and high-alpine regions is challenging and needs an appropriate measurement setup. This was realized by the development and application of a wireless sensor network (WSN) at the Matterhorn field site [*Talzi et al.*, 2007; *Hasler et al.*, 2008; *Beutel et al.*, 2009]. Two distinct features make a wireless sensor network the most suitable measurement system for high-alpine applications: (1) the reduced sensitivity to environmental influences such as lightning, rock and ice fall due to reduction in cabling and (2) the transmission of data from the measurement site in real time. While data are typically analyzed using batch processing the latter might not seem so important yet it has been found that more important than transmitting the sensor data is the capability to analyze the system health and data integrity with very short delay. Especially when compared to traditional data logging equipment this capability allows controlling and reacting upon quality changes in the experimental setup.

[10] In this WSN system autonomous miniature battery powered sensor nodes are fitted with standard commercial and customized sensors. The sensor nodes form an ad hoc wireless network optimized for longevity and reliability. All data are transmitted to a central base station where it is aggregated, time stamped using a UTC referenced clock and sent over a long-distance link to a database server. Furthermore the PermaDozer system used at the Matterhorn site [*Beutel et al.*, 2009] contains storage layers that allow every component to collect and aggregate sensor values autonomously should parts of the system (wireless links, base station, server) be unavailable, e.g., due to weather, snow fall or maintenance.

[11] At Matterhorn Hörnligrat three sensor rods (rigid multithermistor chains), four thermistor chains, two thermistor–moisture chains and eight individual thermistors record rock and cleft temperatures (Table 1). Seventeen crack meters (*ForaPot crack meters, ForaTec*) measure the dilatation and shearing of clefts and in two clefts stress and pressure sensors are installed. The crack meters contain an internal reference temperature sensor allowing compensating thermal errors in the distance measurements. The locations of the sensor nodes are labeled *C* or *R* for cleft and rock respectively followed by a number. At two locations (C6 and C8) two sensors nodes are installed at the same cleft accommodating

Table 1. Site Characteristics and Instrumentation[a]

	Location Description					Sensor Node Description						
		Cleft Size		Orientation		Crack Meters (X/mm)			Temperatures			
Location	Character	Op. (cm)	Ext. (m)	Dir. (deg)	Dip. (deg)	Cr1	Cr2	Cr3	SR	TC	TM	Ts
C1	intense radiation	5 / 0	3	160	80	50			x	x		
C2	concave, wet	15	10	140	85	50			x	c*		
C3	north side	7	6	45	70	150			x	x		
C4	saddle north	3	3	300	80	50			x	x		
C6	top detachment	4	>5	310	90	100	200			x		
C8	large tower	15	40	330	75	100	150			x		
C9	leaning tower	20	20	160	70	100	200	200			c**	
R10	rock south side	free surface		S	90			x		x		
R11	rock north side	free surface		N	70			x		x		
R12	rock large tower	free surface		E	90			x		x		
C20	below C2	5	>5	140	75	100	150					
C21	south low	15–30	20	140	85	100	150					
C22	north low	1	5	310	75	100	150					

[a]Cleft size contains the opening (Op., if not free surface) and the lateral extent (Ext.) of the cleft. The cleft orientation describes the direction (Dir.) and dipping angle (Dip.) of the cleft planes (compare Figure 2). For the crack meters, the numbers indicate the measurement ranges of the present instruments. Temperatures show the type of temperature sensor: SR, sensor rod; TC, thermistor chain; TM, thermistor–moisture chain; Ts, individual temperature sensor measuring the surface temperature (x) or the temperature in a cleft (c* in neighboring cleft, c** in cleft of crack meters).

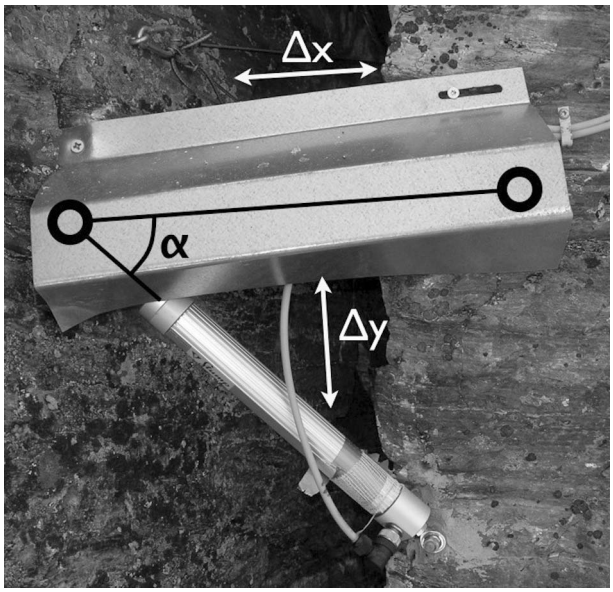

Figure 4. Instrumentation with two crack meters at C8; the crack meter *Cr*1 is hidden under the protection shield and directly measures the dilatation component Δx; the visible crack meter *Cr*2 is used to compute the component Δy parallel to the cleft.

a multitude of sensors, however this is not represented in this labeling for simplicity reasons. For each location the thermistors (or temperature time series) are labeled with *T* followed by a number. Crack meters are labeled with *Cr*1, *Cr*2 and *Cr*3 depending on the number of axes instrumented with crack meters at a given location.

[12] Custom-built sensor rods measure the temperature of the rock at four depths (T1–T4: 0.1, 0.35, 0.6 and 0.85 m) installed in a 1 m deep borehole [*Hasler et al.*, 2008]. Similarly, the thermistor chains and the thermistor–moisture chains measure four to eight temperatures (and on the latter two resistances as an indicator of the presence of liquid water) within clefts (Table 1). The depth of these measurements depends on the installation at each respective location, reaching a maximum of 4 m. Additionally individual thermistors that measure the surface temperature (*Tsurf*) were placed at 2 cm depth in small borings. In two cases, an additional thermistor measures the temperature found within a cleft (C2 and C9 in Table 1). The crack meters are anchored at both sides of the cleft within a distance of some cm from the cleft using chemical anchors and protected by a steel shield against rock and ice fall and excessive solar irradiation (Figure 4). For locations instrumented with a single crack meter only the component normal to the cleft is measured (cleft expansion). By instrumenting a crack with two crack meters the shearing (cleft- and surface-parallel translation, approximately in dipping direction) is measured (Figure 4). As a perpendicular mounting is most likely not possible the actual values are calculated based on the measurement values and corrective angles measured during installation. The sideward shearing is measured by a third crack meter at location C9 but is not considered for analysis here due to the short time series available. Further measurements such as the water pressure and cleft-ice compression stress (perpendicular to cleft surface) could not detect any valuable records so far and as a result was not considered for analysis in this study either. However, the functionality of the pressure measurements was verified and visual inspection confirmed that no ice or water table built up at the position of the sensors. Meteorological data and images from the detachment zone as well as individual instruments are recorded automatically at the nearby base station [*Beutel et al.*, 2009]. The meteorological data recorded cover only a limited time span as will be explained later, do not include snow precipitation, and were mainly used to check the validity of an extrapolation of precipitation events from the meteorological station in Zermatt.

3.2. Measurement Locations

[13] The general characteristics of the measurement locations are described in Table 1. In the following the spatial relation of the individual locations is briefly described (see also Figure 1): All clefts instrumented with crack meters except for C3 are running parallel to the ridge (family A, Figure 2). The cleft of C1 cuts across the detachment surface (Figure 3). It is approximately 2 m deep and 4 m long and exposed to strong solar radiation. In summer 2010 the position of the crack meter located at this cleft was changed from crossing the cleft to a position not crossing the cleft to determine the accuracy and repeatability of an instrument mounted on a portion of solid rock, i.e., at a known non-moving position (see below). Sensor C2 is located in the corner of the detachment (Figure 3) and measures one of a series of clefts with debris and clay infill. The upper part of this corner accumulates snow during winter. At the top of the detachment zone sensor C6 monitors a cleft, which divides the ridge with thermal influence coming from both sides of the ridge. Figure 3 also shows C20 located in the lower left part of the detachment surface at a cleft parallel to the one of C2. On the north side of the ridge C3 and C4 are installed in proximity of the detachment zone (Figure 1). The cleft of C3 is perpendicular to the other clefts and divides the northwestern rock flake of the steep ridge limiting the detachment.

[14] The crack meter C8 and a sensor rod (R12) are located at the northeasterly oriented face of a tower 50 m northeast of the detachment zone (Figure 1). This tower is divided by a big cleft that extends to a depth of about 40 m. C8 is installed across this cleft at 8 m from the top and R12 is drilled into compact rock at 4 m from the top to record the temperature evolution in this rock mass. Two other sensor rods are installed on both sides of the ridge between the tower and the detachment zone to survey the thermal conditions found in a southeasterly exposition (R10) and a northwesterly facing cliff (R11). Their distances to the ridge are 15–20 m, hence more than 20 m rock mass lie between both sides and reducing the effect of large lateral heat fluxes in the ridge [*Noetzli et al.*, 2007] on the temperature profiles recorded.

[15] Additionally, on both the north and south sides of the ridge a cleft is instrumented at a larger distance away from the ridge and the detachment zone: The location C21 is on the south side at a large cleft separating a 20 m high and 7 m thick rock mass from the slope (Figure 1). Water is supplied from the melt of a snow patch above and seasonal ice is observed close to the surface in this cleft. Tilted blocks at the top of the cleft indicate an outward movement of the rock

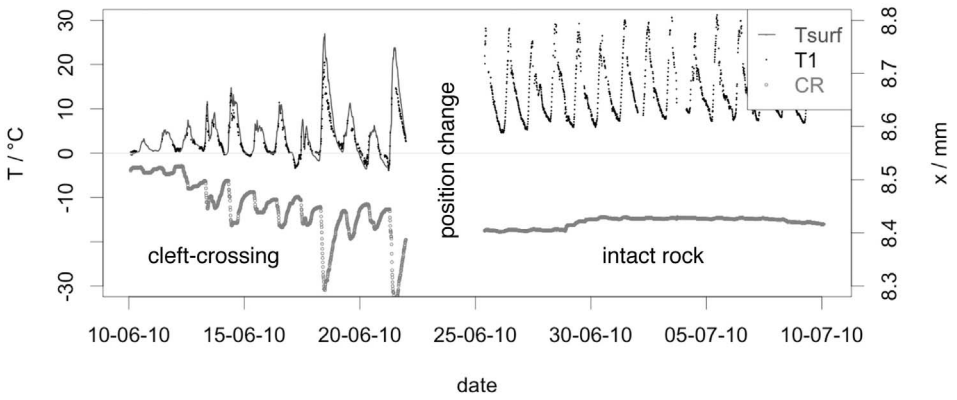

Figure 5. Validation of crack meter measurements at C1. Time series of rock surface temperature (*Tsurf*) and top cleft temperature (*T*1) and crack meter expansion *(CR)* for the instrument installed across the cleft (June) and in intact rock (July).

mass. Since no cleft of the same extent as at C21 was found on the north side, C22 is installed at a similar situation but with smaller cleft dimensions. Sensor C22 is located 40 m from the ridge in the north face. In contrast to the south side, no geomorphic indications of large movements exist here and the water supply is smaller due to the thermal conditions and geometric settings. Finally, a last sensor C9 is installed 100 m above the detachment zone at a tower located in the southeast face (Figure 1). This tower apparently leans toward the ridge. A niche from a small rockfall is visible at the tower basement forming an overhang. The southward dipping cleft (C9 in Table 1), dividing the tower from the face, is instrumented with three crack meters to resolve for all three axes. Its topographic position on a spur prohibits the supply of larger quantities of meltwater.

3.3. Data Quality

[16] The reliability and quality of the expansion and shearing time series measured is essential for the interpretation whereas the measurement accuracy of the temperature measurements is less critical because in our context the main uncertainty arises from high spatial heterogeneity. It is thus sufficient to state that the absolute accuracy requirement for the temperature measurements is ±0.2°C [*Hasler et al.*, 2011a].

[17] The test setup for the crack meters is similar to the one by *Matsuoka* [2001a]: Both anchor points of the instrument at location C1 are mounted on intact rock without a cleft in between (except for one micro fissure) and the movements measured by the instrument are analyzed. These data are compared to results from the same crack meter mounted across a cleft prior during an earlier period in time revealing the effect of changing temperatures on the rock mass and instrument respectively (Figure 5). The expansion-temperature relation (dx/dT) measured for the cleft-crossing installation (Cr1 and T1 data measured before 25 June 2010) is −10 μm/°C. The same relation measured for the intact rock installation (after 25 June 2010) is +0.2 μm/°C, but with a lower correlation because of shifts found between different periods following this trajectory (Figure 5). The typical linear thermal expansion coefficient for crystalline rock is in the order of $5 \cdot 10^{-6}$/°C, which means that the expansion of a rock mass of the size between the anchor points (150 mm) is approximately +0.7 μm/°C. The lower expansion measured (+0.2 μm/°C) agrees well with this theoretical value because the rock at the surface needs to deform elastically constrained by against the lower rock masses with less (diurnal) temperature amplitude inducing thermal stresses preventing free deformation. The shift of the crack meter extension on intact rock (Figure 5) may originate from inelastic distortion and stress field variations on a larger scale. This result indicates that the internal temperature compensation of the crack meter works well and a relative measurement accuracy of better than ±0.1 μm/°C can be assumed resulting in an absolute crack meter accuracy of ±5 μm over a temperature range of 50°C and across a measurement range of 50 mm. An elongation of the crack meter from 50 to 200 mm range results in a linear decrease of the total accuracy of ±20 μm, which is well below the signals anticipated. On the multidimensional measurements, the accuracy of the movement component Δy parallel to the cleft may be lower than Δx perpendicular to the cleft because it is calculated by subtraction (error propagation) and depends on the angle between the two crack meters (α in Figure 4): We assume an accuracy of Δy of ± 100 μm for all sensors except for C6 (err.Δy = ± 12 μm; α = 90°).

[18] Consistent time series of data from the sensors initially installed in 2007 (C1–C8 and R10–R12) start in July 2008. Prior to this date only fragmentary data from early tests exist which are not used in this study. From July 2008 to November 2010 the data set has several gaps due to technical problems (Figure 6). In the summer of 2009 a data gap over a period of two months is a result of a breakdown of the WSN due to a software error. The crack meter measurements at location C4 are only available from the summer of 2010 onwards due to mechanical damage to the sensor that was only discovered then. Another substantial gap is the one of location C6 in the spring of 2010. The sensors installed during the extension of the field site in June 2010 (C9, C20–C22) have delivered continuous time series since except for location C9, which contains two small gaps in autumn 2010. The values of crack meter C8, experienced a

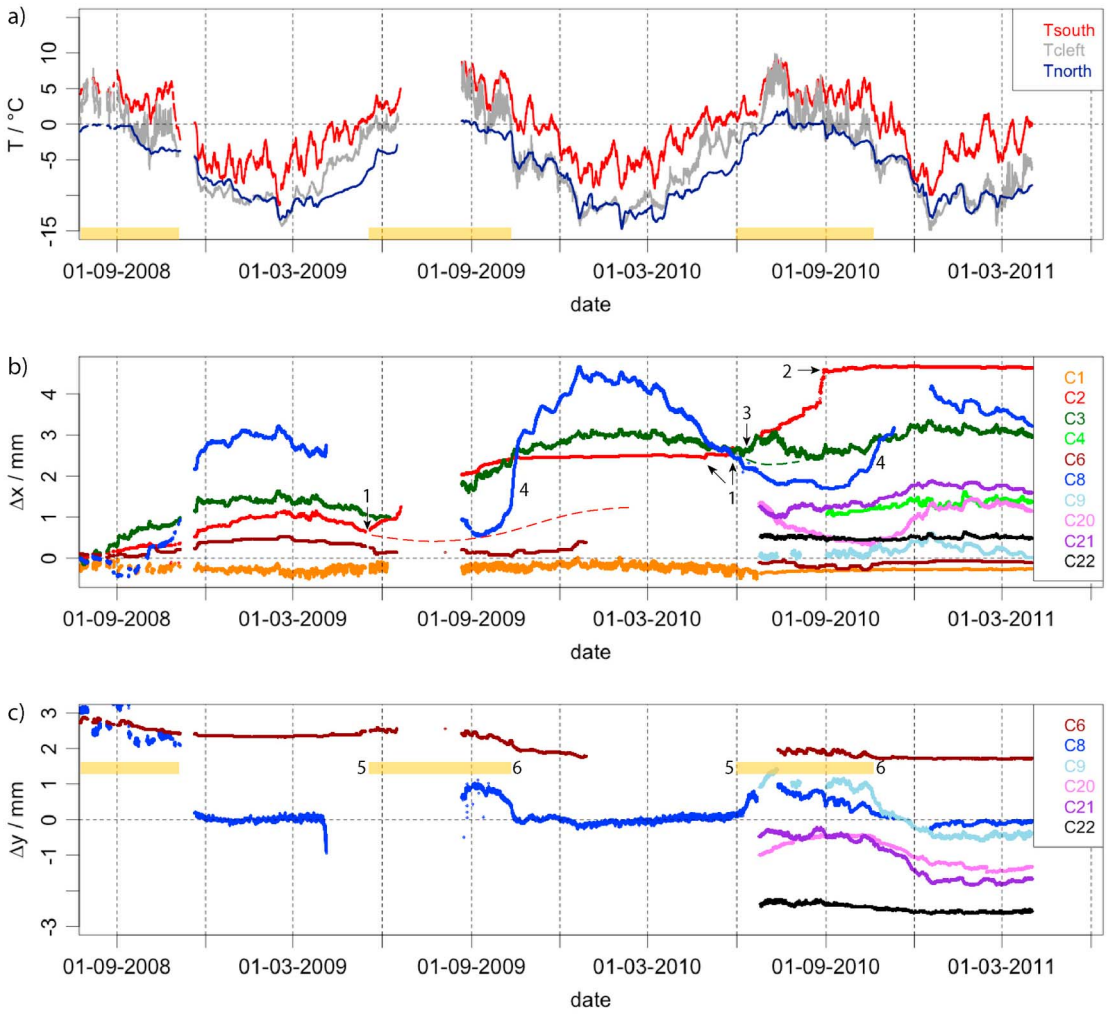

Figure 6. Overview of thermal conditions and cleft movements at the Matterhorn Hörnligrat showing patterns negatively correlated with temperature during the cold season and enhanced shearing in summer. (a) Rock temperatures on southeast and northwest side at 0.85 m depth and cleft temperature at 2 m depth. The yellow bars indicate $Tcleft \geq 0°C$. (b) Cleft expansion Δx. (c) Shearing Δy with positive signs for upward movement of the valley-side rock mass (see Figure 4). The numbers indicate events of special interest that are described in the text.

bias due to a short circuit in another sensor attached to the same sensor node that was disassembled upon detection of this problem in June 2010. Analysis revealed the main problem to be a drop in the reference voltage that could be corrected by multiplying the raw values by a factor of 2.1 of the crack meter time series of location C8 prior to June 23, 2010. The behavior of the data of location C8 prior to the data gap in summer 2009 could not be explained satisfactorily and so these data are not considered for the analysis.

[19] The on-site meteorological time series cover autumn 2009 and summer 2010 and detailed image data is available from pictures automatically taken several times per day over large parts of the whole measurement period.

[20] All the data are sampled every 2 min and aggregated to 10 min averages as a base for the analysis presented here. This aggregation produces deviations smaller than 0.1°C from the instantaneous raw values even for signals with a large short-term variation.

4. Results

4.1. Rock and Cleft Temperatures

[21] The temperature measurements in clefts and shallow rock boreholes show differing diurnal and annual amplitudes depending on their location and depth. In order to illustrate the seasonal temperature evolution at the field site three temperature time series from the bottom of the shallow boreholes and clefts are presented in Figure 6a. This data however conceals the fact that the diurnal temperature fluctuations at the rock surface at locations exposed to direct solar radiation exceed the amplitude found in the annual fluctuations (e.g., Figure 5). The difference between the rock

temperatures southeast (T4 at R10) and northwest (T4 at R11) of the ridge is approximately 6°C on average (Figure 6) with a mean annual ground temperatures (MAGT) of 0°C and −6°C respectively. The temperature data derived from the southeast aspect has larger weekly amplitudes with the two temperature curves running almost in parallel with respect to annual fluctuations. The cleft temperatures (C6-T4) have larger annual amplitudes with strong diurnal signals found in some time periods (Figure 6). This is observed for all measured clefts even though the extent of periods with large diurnal fluctuations varies with the cleft location and measurement depth within this specific cleft. This variation in diurnal amplitude reflects that the recorded cleft temperatures are a mix of air temperatures, rock surface temperatures in the cleft and the temperature of a possible cleft infill (snow, ice, water and debris). Therefore, the imprecisely defined physics of the measurement setup in the cleft and the varying conditions need to be considered here: The accuracy of the data is reduced by a possible bias introduced by the setup (e.g., conduction along cables, ice formation on sensors) inherently difficult to quantify. On the other hand, the high correlation found in data derived from several temperature sensors mounted within a single cleft ($r > 0.86$ for all cleft temperatures) demonstrates that an interpretation with respect to the thermal evolution of the cleft can be performed. For the detailed analysis of the cleft movements the temperature with the highest correlation to the expansion at the respective cleft is adopted within this study. These are the surface temperature for cleft C1 (C1-Tsurf), the temperature at 0.5 m depth for cleft C2 (C2-T6) and for cleft C3 the one at 0.6 m depth (C3-T4). The movements at C8 are analyzed in relation with the rock temperatures at 0.85 m depth (R11-T4).

4.2. Cleft Kinematics

4.2.1. General Patterns of the Cleft Expansions

[22] An overview of all measured cleft movements is provided in Figures 6b and 6c. The illustration 6b shows expansion relative to the initial values of each data series allowing a joint visualization and not the total aperture of the cleft given in Table 1. For the first year (July 2008 to June 2009) all cleft expansions show a negative dependency on temperature but with differing amplitudes and attenuation over time: A negative correlation with the annual temperature evolution prevails at C2, C3, C6 and C8 (Figure 6b). The peak-peak values of these annual amplitudes are in the range of 0.5 to 4 mm. In contrast, C1 shows diurnal cycles with amplitudes of about 0.2 mm (see also Figure 5). Equally, at C3 and for a limited time between February and April 2009 at C2 short-term cleft movements overlay the lower frequency signals of the annual cycle. After the data gap in summer 2009, these general patterns are visible again except for C2, which almost stagnates during the entire winter after leaving the expected negatively temperature-correlated path (dashed red line in Figure 6b). Of the five clefts with measurements available for more than two years, three clefts (C2, C3 and C8) experience net-expansions in the order of 1–2 mm/a; at C1 and C6 the expansions are reversible. The irreversible openings were composed to large parts by deviations from the observed negative dependency occurring in summer (C2, C3) or an enhanced opening during the freezing period (C8). Both periods are described and discussed in more detail below. The sub-annual time series from the sensors installed in June 2010 adumbrate the following: (1) the negative dependencies on temperature during winter was similar to the ones of the other clefts; (2) during summer and autumn these dependencies varied between locations (different delays); and (3) C22 in the north face showed a minor dilatation.

4.2.2. Cleft Shearing and Two-Dimensional Movements

[23] For the shearing motions, a seasonal difference is evident: In the long shear time series from C6 and C8, significant activity was limited to the warm periods. At C6 the active time span was from May to mid-October in the year 2009 and stopped at about the same date in 2010 (Figure 6c, 5 = start, 6 = stop). The values however stagnated with an offset found between successive winters. The shearing of the cleft at location C8 stopped at the same time in both years (the start could not be evaluated for the year 2009). In contrast to C6, the shearing component in C8 returned to the same position in the two autumns. A direct comparison of the timing of this activity is not possible due to diverse gaps in the two data sets (Figure 6c). The shearing time series of C9 and C21 show large movements in summer and autumn and rather constant values in winter while at C22 only minor shearing activity was observed (Figure 6c). The shearing at C20 followed the annual temperature fluctuations with a delay (positively temperature-correlated).

[24] In Figure 7 the 2-dimensional movement patterns of C6 and C8 are shown. The two components correspond to the dilatation (cleft-perpendicular) and the shearing in the (near-) dipping direction (Figure 4). As both clefts are near-vertical and the shearing is plotted on the ordinate, the graphs can be interpreted as the translatory movement of the rock mass relative to the other side of the cleft (compare sketches in Figure 7). In case of C6 the relative movement of the southern block is plotted and for C8 for the northern block with the colors signifies the cleft temperature. The transition from shearing to opening was similar for both cases but the inter-annual offset is larger on the y axis for C6 and on the x axis for C8. This indicates, that the cleft at C6 had a small trend in shearing (<0.5 mm/y), while C8 had a trend in opening (1–1.5 mm/y).

4.2.3. Summer Expansions

[25] At C2 the non-reversible movement was composed of two expansions of 2 mm each that occur in summer when the cleft temperature was at or above 0°C (Figures 6a and 6b). The temperature dependency of this summer expansion deviates visibly from the negatively temperature-correlated expansions described above. This second movement mode started in early summer when thawing occurred inside the clefts (Figure 6b, 1) and abruptly stopped with the first freezing at the end of August (Figure 6b, 2). In 2010 a first melt event led to some expansion but continued expansion was initiated with a second melt period followed by sustained positive cleft temperatures. Figure 8 shows a detailed time series of this summer expansion and cleft temperatures at C2. The start of this expansion was simultaneous with the first significant positive temperatures measured at the top of this cleft. With a delay of four days the temperatures within the cleft reached 0°C and remained at or above this temperature for the most part of the following three months (Figure 8; for the gap compare Figure 6a). The movement mode was a stepwise expansion (motion time < minutes) with plateaus found in between. The steps occurred in the afternoon in most

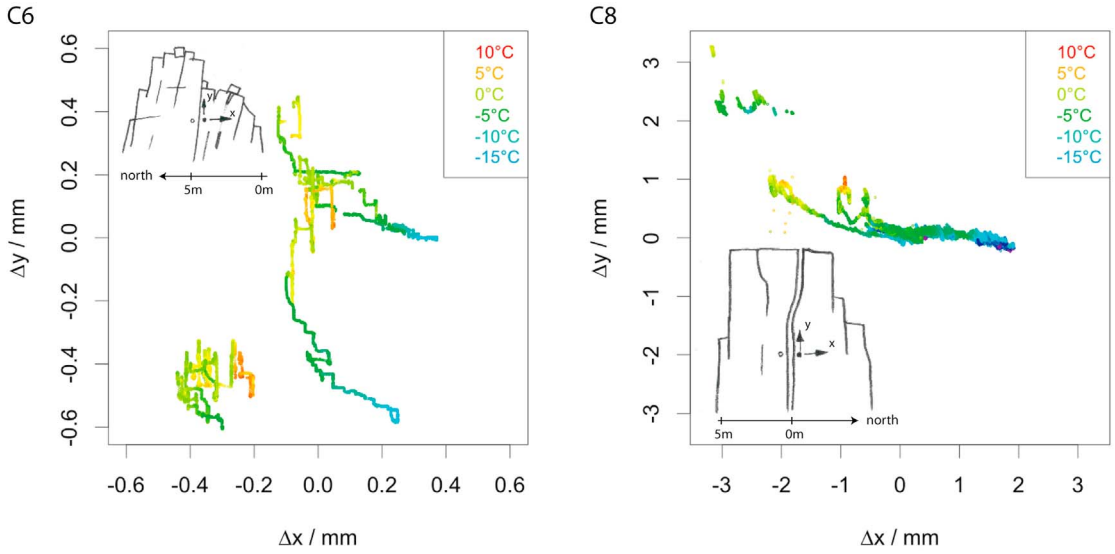

Figure 7. 2D-movement pattern with cleft temperature (color) at C6 and C8. The shearing component Δy is the position of the right mass relative to the other side of the cleft.

cases (78% of the 32 distinct steps that are larger than 0.01 mm). There is no correlation of the steps with the timing of significant precipitation events (Figure 8). A significant increase in the number of steps occurred at the end of August before cleft freezing terminates the movement (Figure 8). In Figure 9 the cleft expansions are plotted against the temperatures found within the clefts. The partly reversible expansion for C2 of the winter 2008/2009 was not repeated in the following winter with the whole opening process found in this cleft occurring while the cleft temperature at 0.6 m depth was larger than 0°C (Figure 9, C2). The minor dependency of the cleft expansion on the positive temperatures is illustrated in Figure 9 by the horizontal stripes that are shifted upward (offsets of the trajectories) when steps occurred. No dependency between the expansion rate (dx/dt) and the temperature could be determined.

[26] During the data gap of the summer 2009 an expansion occurred at C3 continuing during the freezing period of the north side in September (Figures 6a and 6b). An opening in summer 2010 showed a deviation from the negative correlation with the cleft temperature typically found (Figure 6b, C3 and green dashed line) and being reversible in contrast to the situation at C2. The transition from the negative to positive temperature-correlation occurred around mid-June but without a visibly abrupt regime change (Figure 10). It ended with a temperature drop in the cleft on 24 July. The diurnal fluctuations remain negatively correlated with diurnal temperature variation for the entire warm period. The movement

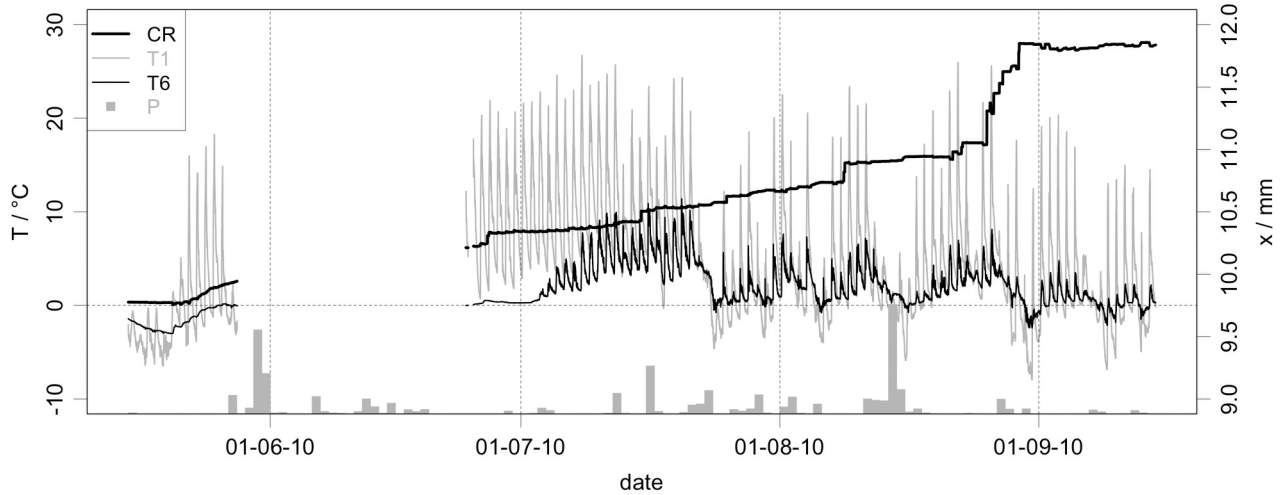

Figure 8. Cleft expansion with stepwise opening at C2 in summer 2010 and corresponding cleft temperatures. *CR*, the crack meter expansion; *T*1, temperature at cleft top; *T*6, 0.6 m depth; *P*, diurnal precipitation in Zermatt (qualitative indication: maximal value is 62 mm).

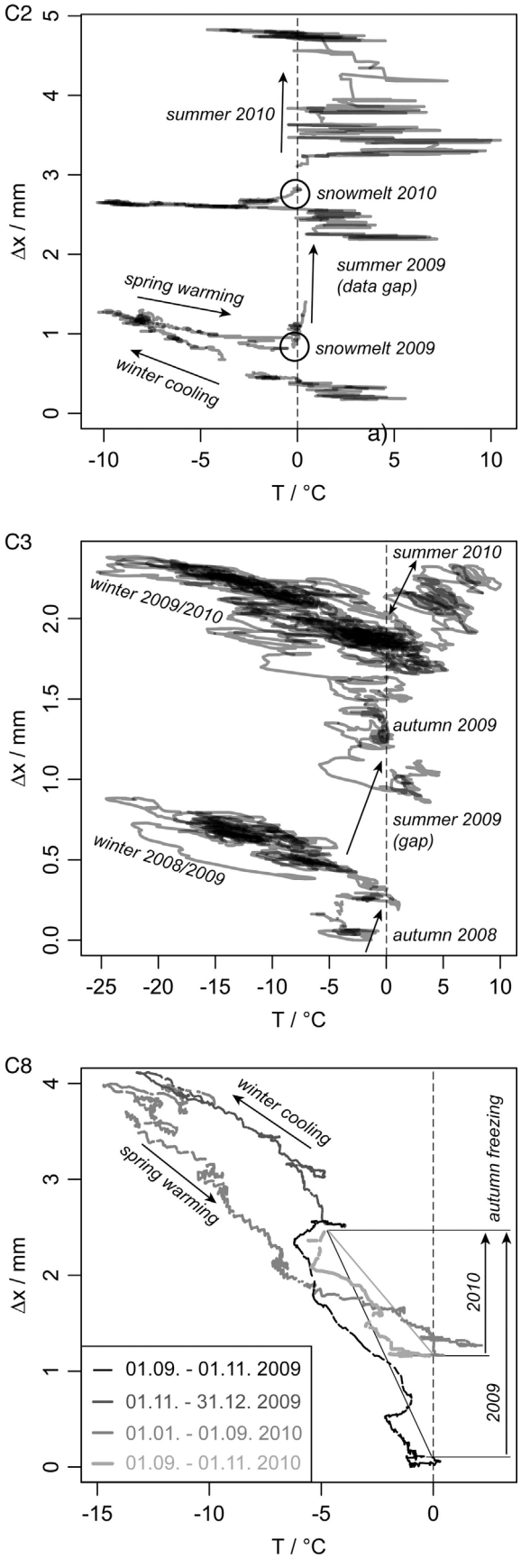

Figure 9. Cleft expansion as a function of temperature $\Delta x(T)$ at C2, C3 and C8. For C2 the correlation between Δx and the plotted cleft temperature $T6$ (0.6 m depth) has a Pearson's coefficient of $r = -0.95$ for the first winter. For C3 the correlation between Δx and $T4$ (0.5 m) has an $r = -0.82$ for winter 2008/2009 and an $r = -0.84$ for winter 2009/2010. Δx of C8 is plotted against the rock temperature $T4$ (0.85 m) of R11 and has an $r = -0.91$ over the whole time span. The lines are transparent to visualize overlapping; for C8 the line style varies by period (legend).

mode was continuous without steps such as those found at C2 (Figure 10). In the diagram showing the expansion versus temperature (Figure 9) this behavior does not lead to an offset and the trajectories being generally negative inclined.

4.2.4. Autumn Freezing Period

[27] The major opening events in the data (except the summer opening) coincide with a rapid temperature drops (Figures 6a and 6b). Noticeable are the expansions at C8 during the initial autumn freeze periods of 2 and 1 mm each, occurring within a few days (Figure 6b, 4). A comparison of the two opening events in 2009 and 2010 is shown in Figure 11. The initial aperture at the beginning of September differed by 1 mm only between the two years. The cleft temperature evolution in 2009 was characterized by values that remained around 0°C until October 10th and then dropped by 10°C within just a few hours. In the following two weeks the temperature fluctuated around −10°C (Figure 11). The temperature drop in 2010 was less sudden. A first intense freezing event occurred already end of September, followed by slightly positive temperatures before the temperatures finally decrease below zero degrees (Figure 11). The difference in expansion and expansion rate between these two periods is not proportional to the slight difference observed in the net temperature decrease for these two years. Despite the dependency of the cleft expansion on the lower rock temperatures (Figure 11) the expansion-temperature relation was not constant over time and shows a path dependency (Figure 9). In 2009 a larger gradient is visible in the expansion-temperature relation than in 2010. For the other clefts a clearly increased expansion during autumn freezing was not observed.

5. Discussion

5.1. Measurement Patterns and Correlations

[28] Based on the preceding description of cleft kinematics, we identify two main regimes of movement. The first one persists for most of the year and at some locations is replaced by the second regime for a variable period (a few weeks to months) when the cleft temperatures are above 0°C. In the following discussion we call these (1) the temperature-correlated dilatation regime and (2) the enhanced expansion and shearing regime. While the temporal extent of these periods differs between the clefts, their general characteristics and relation to temperature are similar and discussed below.

5.1.1. Temperature-Correlated Dilatation Regime

[29] This period is characterized by the predominance of a negative correlation of the cleft expansion with temperature. It occurred at all clefts during winter except at C2 where the

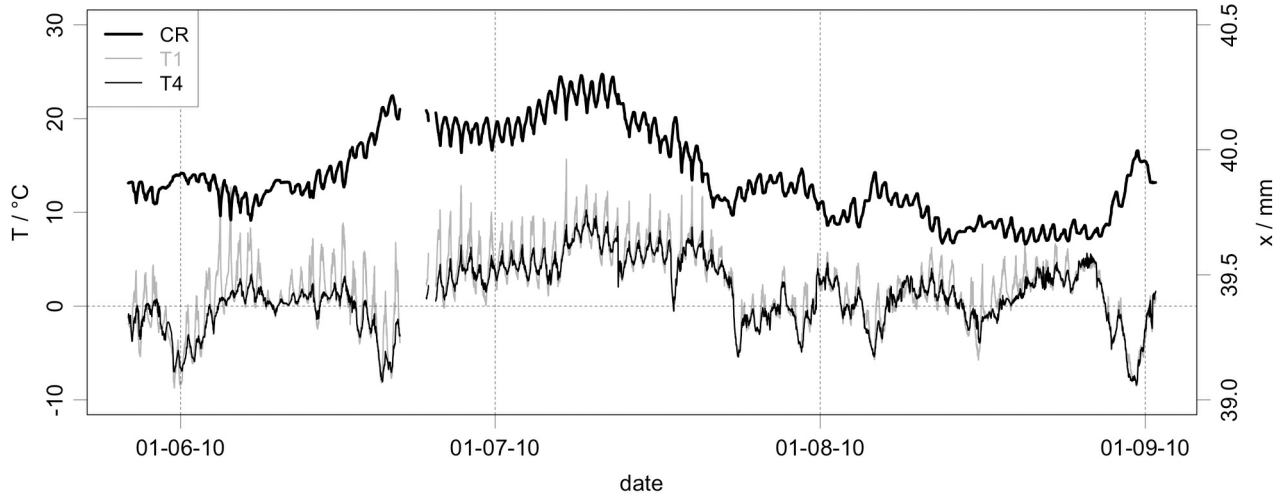

Figure 10. Cleft expansion and cleft temperatures at C3 in summer 2010. *CR*, crack meter expansion; *T*1, temperature at cleft top; *T*4, 0.5 m depth. End of June the cleft expansion changes from negatively temperature-correlated to positive dependency from temperature for one month.

negative correlation was limited to the winter 2008/2009. The thermal cleft expansion gradient dx/dT differs between locations and shows variations both over time and with the path direction (opening/closing). Table 2 presents an overview of these gradients. The basis of these gradients is a qualitative interpretation of the expansion versus temperature plots and a regression analysis performed between these two variables (see Figure 9 for C2, C3, and C8). The Pearson's correlation coefficient for the two cleft dilations C1 and C6 is $r = -0.85$ (Δx versus *Tsurf*) and $r = -0.38$ (Δx versus *T*4). The gradients span almost two orders of magnitude and correspond with the annual amplitudes. At C8 where the cleft dimension is bigger than at the other clefts (see Table 1) the gradient was largest. At C1, the cleft which is smallest in dimension, the least temperature dependent dilatation values were recorded. However, the gradients at the clefts C2 and C6 should not be mistaken as the relative lateral movement of the larger rock mass because here only one cleft within a series of clefts was actually measured. For the interpretation of the larger movements at C8 we have to consider that (1) the measurement location was situated above the root zone of the cleft in a large tower and hence the signal measured may be amplified relative to its origin by a tilting component (see sketch in Figure 7) and (2) the exceptionally large gradient of 0.5 mm/°C was restricted to the freezing period of autumn 2009 (Figure 9).

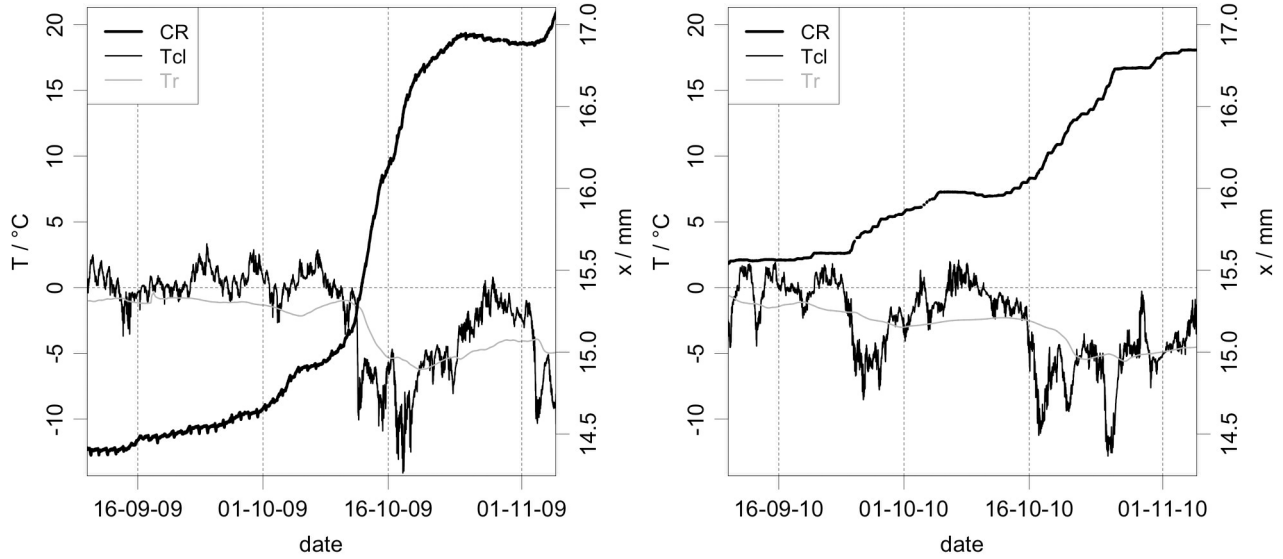

Figure 11. Cleft expansion at C8: comparison of 2009 and 2010 autumn freezing. *CR*, crack meter expansion; *Tcl*, cleft temperature in 2 m depth at C8; *Tr*, rock temperature in 0.85 m depth on the north side (R11).

Table 2. List of Average Gradients of Cleft Expansion Gradients

Sensor	Expansion Gradient (mm/°C)
C1	−0.01 (diurnal fluctuations)
C2	−0.1 (opening), −0.05 (closing; 2008/2009)
C3	−0.02 to −0.04
C6	−0.04 mm/°C (with no sensitivity on T in between)
C8	−0.2 (general), −0.5 (freezing 2009), −0.3 (freezing 2010)

[30] Characteristic for all measurements is the absence of significant shearing, a fast reaction to changes in near-surface temperature and a continuous movement mode during the negatively temperature-correlated dilatation regime. At a seasonal scale this correlation exists with regard to the temperatures at depth or a smoothed surface temperature with a minor dependency on short-term temperature fluctuations existing at some locations. This leads to the assumption that one could describe the cleft dilatations observed with a regression model that considers short-term variation and long-term evolution of the near surface rock or cleft temperatures. Modification of the crack meter regression model of *Nordvik et al.* [2010, equation 6] with a temperature record that reflects the seasonal variations (taken from depth or smoothed) instead of a sinusoidal explanatory function, may reveal a larger temperature dependence of cleft movements. Different time series analysis, such as the cross correlation function or a correlation analysis of the two signal decompositions of temperature and cleft expansion, may be able to quantify these dependencies and their variation over time in more detail - once longer time series of data are available.

5.1.2. Enhanced Expansion and Shearing Regime

[31] In subsection 4.2 two main features are described that we subsume under this regime. The first is the summer expansion that is initiated by isothermal/positive temperatures in clefts and the second is the enhanced shearing. In summer the cleft movement departed from the characteristic path of the negatively temperature-correlated dilatation regime in one of the components of the cleft movement. In 2010 this became visible between end of May and mid-June for all

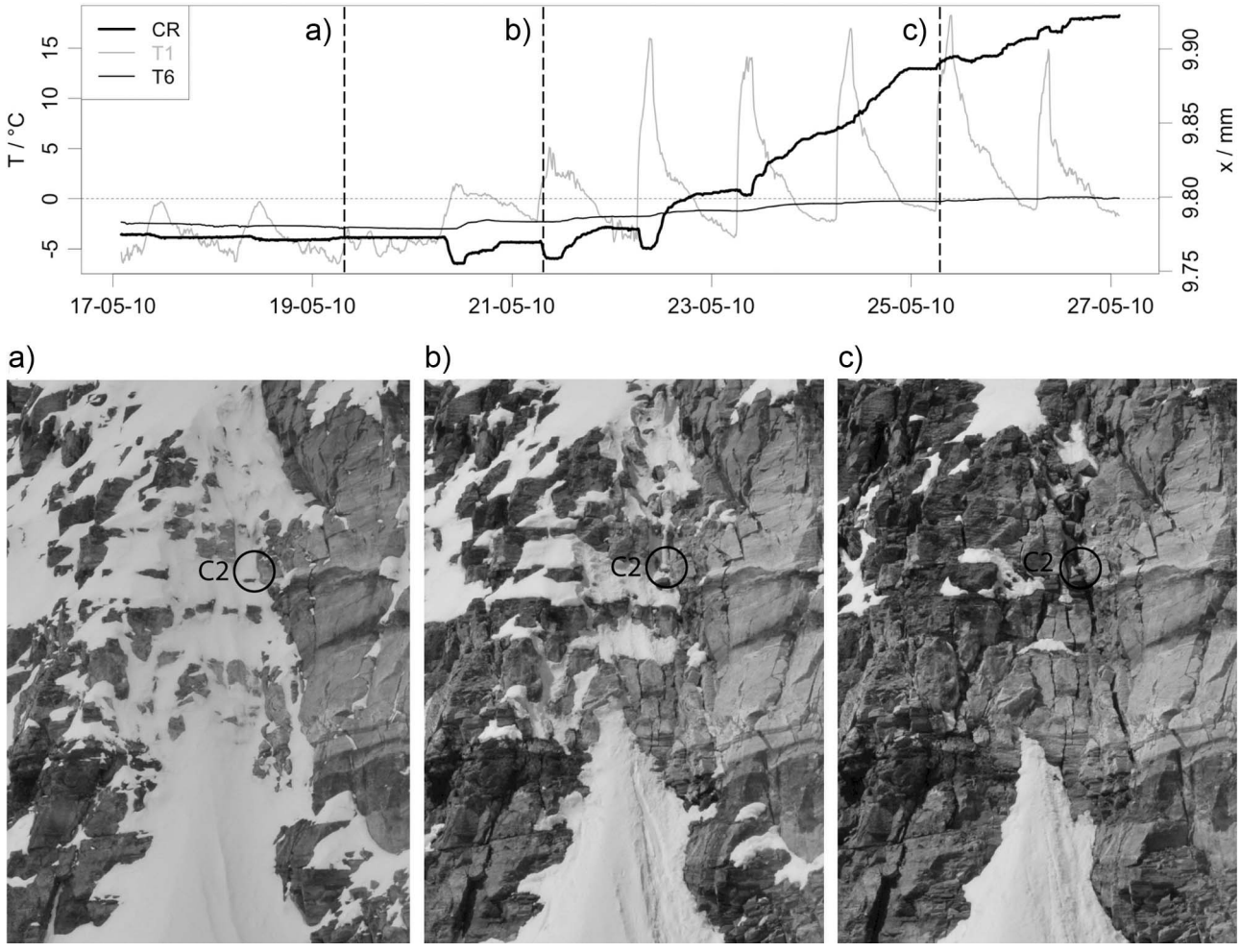

Figure 12. Transition to snow free conditions in the detachment zone around C2 during initial melting 2010. The time series with crack meter expansion (*CR*) and temperatures (*T1*, *T6*) from C2 contains indications (a–c) of time when pictures are taken. (a) May 19th, 9:45 A.M.; (b) May 21st, 8:45 A.M.; (c) May 25th, 8:45 A.M. *T*1 is measured at cleft top; *T*6 at 0.6 m depth.

locations subject to this regime. Figure 12 illustrates the coincidence of this behavior with snowmelt for C2. Mostly snow-free conditions in spring 2010 were first reached at the end of April with subsequent snow fall leading to a temporal extent in snow cover (Figure 12a). On 21 May some last snow patches remained in clefts, but disappeared over the next couple days. Simultaneously, cleft temperatures rose up to 0°C and summer expansion commenced (Figure 12). At C6 the reaction of the cleft temperatures to the snowmelt near the surface was observed ten days later. At the same time the shearing activity started at C8 and the transition to summer expansion took place at C3 (Figure 6). The regime change is clearly identified before the summer maxima of the exceptionally warm period of July 2010. The highest activity of the stepwise opening of C2 was observed after this warm period and no coincidence of such opening events with precipitation was found (see section 4 and Figure 8). The retardation of snowmelt a few days after precipitation possibly masks a dependency between precipitation and opening activity. For the large movements at the end of August (Figure 8) such a connection to recent precipitation is unlikely because the last snow fall had occurred 12 days before. A spatial interpretation of the movement and its extent at C2 was not possible because the cleft movement was only measured in one dimension. The upward shearing of the lower cleft (C20) in July and August can be possibly attributed to a toppling movement of the southern rock mass.

[32] So far we have stated patterns and correlations, but not causal relationships between the thermal, hydrological and meteorological conditions described and the cleft movements. In the following, we discuss possible explanations for the two regimes and formulate hypotheses about which (combination of) physical mechanisms described in literature could explain the phenomena observed.

5.2. Hypothesis 1: Thermomechanical and Cryogenic Forcing of Cleft Dilatations

[33] Cleft expansions that are negatively temperature-correlated have been observed at various permafrost sites [*Wegmann and Gudmundsson*, 1999; *Matsuoka*, 2008, 2001a; *Nordvik et al.*, 2010] and at some rock slopes in non-permafrost areas [*Watson et al.*, 2004; *Gischig et al.*, 2011b; *Mufundirwa et al.*, 2011]. For permafrost bedrock, ice formation processes (cryogenic processes) such as ice segregation [*Wegmann and Gudmundsson*, 1999] or the volumetric expansion of bulk freezing of cleft water [*Matsuoka*, 2001a] have been inferred as the driving processes of these movements. In contrast, the opening during cooling and stagnation or re-closing during warming is attributed to elastic deformation of rock due to stress caused by the thermal dilatation of near-surface rock layers (thermomechanical forcing) [*Watson et al.*, 2004; *Gunzburger et al.*, 2005; *Gischig et al.*, 2011a]. We postulate a combination of these physical processes to explain the observed negatively temperature-correlated cleft movements because none of the processes suffice individually.

[34] *Wegmann and Gudmundsson* [1999] assumed ice segregation as the explanatory process based on the correlation between borehole extensometer strain rates (dx_{Ex}/dt) of fractured rock and a calculated freezing rate in the corresponding temperature profile. Significant freezing rates found for positive rock temperatures [see *Wegmann*, 1998, Figure 8.2] justify some suspicion and point to a shortcoming in their method: The calculation of the freezing rate is especially sensitive to thermal parameter estimation if large temperature gradients ($|dT/dt|$) occur. Possibly, the postulated dependency of the strain rate on the freezing rate only results from the inherent correlation between dT/dt with the strain rate (or the cleft expansion rate) of the negatively temperature-correlated regime. However, for porous sedimentary rock, ice segregation has been proven as the driving process for rock fracturing, ice lens formation and corresponding frost heave in laboratory experiments [*Akagawa and Fukuda*, 1991; *Murton et al.*, 2001]. With the low permeability of (frozen) crystalline rock and a cryogenic suction of about 15 kPa [*Fukuda*, 1983] we cannot explain the fast reaction of cleft movements to the surface temperature changes observed by a segregation process. This is supported by the fast response of micro-seismic activities on rapid temperature drop recorded at another permafrost site at the Matterhorn [*Amitrano et al.*, 2010]. Furthermore, the negative temperature dependency at strongly negative or positive temperatures does not correspond to the pattern of ice segregation (compare to *Matsuoka and Murton* [2008, Figure 6]) and the water supply for a long-term cleft ice growth (mm to cm) through meters of frozen rock is limited by low permeability and hydraulic gradient. *Matsuoka* [2001b] discussed this discrepancy between laboratory experiments with porous sedimentary rock and the field conditions in hard, fractured rock. He argues that the hydraulic and thermal conditions differ strongly between clefts and the inter-cleft rock masses and therefore, laboratory results cannot simply be applied to the widening of pre-existing macrofractures. The coincidence of short-term cleft expansion and freezing at the cleft top of clefts 2–5 mm wide in the Japanese and Swiss Alps where attributed to freezing-induced volumetric expansion on the order of 9% instead of ice segregation [*Matsuoka*, 2001a, 2008]. Here one part of the negatively temperature-correlated cleft expansion may be attributed to a similar process, the exceptional large opening during autumn freezing (e.g., C8). This however requires the retentions of liquid water within the cleft prior to freezing. Even though a hydrologically closed situation is unlikely for large clefts, cleft infill (debris and clay or snow) might serve as a retention substrate. Volumetric expansion (and possible ice segregation within the cleft infill) during freezing progression can cause expansive stress on the cleft walls and support opening.

[35] To explain the seasonal and also the short-term cleft expansion from the Matterhorn, the concept of a thermomechanical forcing is more convincing. This concepts explains the negatively (and positively) temperature-correlated movements across discontinuities by the thermal expansion and contraction of near-surface inter-cleft rock masses [*Watson et al.*, 2004; *Gischig et al.*, 2011a]. This thermally induced stress and reactive (cleft-) movement propagates several tens of meters into the rock to depths where only minor annual temperature fluctuations exist. The particular trajectories and possible amplification of such relative cleft movements, depend on the geometric (topographic and structural) settings that mask the influence of gravity together with the mechanical conditions of the clefts. Despite the variation of these parameters from site to site and

corresponding differences in the reversibility and phase of the recorded movements, common annual temperature dependent patterns point toward similar driving processes. *Gischig et al.* [2011b] applied coupled thermal mechanical finite element models for compact and fractured rock to reproduce deformation from a post-failure rock slope in Randa (Swiss Alps). With respect to this approach an important characteristic is the absence of high variations in water pressure within the cleft system, which would modify the stress normal to the cleft and change the effective friction. The absence of high (variations in) water pressure reveals the temperature dependency of the movements because in this case they are not dominated by rock hydrology. Similar vadose hydrological conditions were observed by *Watson et al.* [2004] in an unstable rock slope at Checkerboard Creek (Canada) showing temperature dependent movements. The lack of liquid precipitation during most of the year and partial ice sealing of clefts may lead to analogue reactions of many permafrost areas to temperature fluctuations.

[36] Therefore, we hypothesize that the negatively temperature-correlated regime of the cleft dilatations presented here is caused by thermomechanical forcing and that the additional (enhanced) expansion in autumn is caused by ice formation processes in a substrate that retains liquid water. A similar combination of thermomechanical forcing and ice formation is known to be the driving mechanism for the formation of ice-wedge polygons in arctic permafrost [*Lachenbruch*, 1962]. These two processes differ with respect to the timing of ice formation and the influence of gravity. However, the example of ice-wedging illustrates the importance of ice formation in combination with thermally induced movements. Ice formation prohibits a re-closing by its frozen cleft infill and causes an inter-annual accumulation of movements even if the geometric setting would lead to reversible movements.

5.3. Hypothesis 2: Hydrothermally Caused Shear Strength Reduction

[37] The regime of enhanced opening (C2, C3) and shearing (C6, C8) cannot be plausibly explained by Hypothesis 1; it contradicts the general trend of cleft contraction in summer following the negative temperature-correlation. Furthermore, a higher cryogenic activity due to meltwater supply in the clefts, analogous to the summer frost heave in porous rock [*Murton et al.*, 2001] or spring freezing expansion [*Matsuoka*, 2008], would limit itself after a few days due to the concentrated release of latent heat along the cleft – resulting in local warming [*Hasler et al.*, 2011b]. As an alternative explanation, we suggest a change in the resistive forces against gravity and thermally induced stress.

[38] According to the formulation of Terzaghi, stress in hard, fractured rock acts on discontinuities and intermediate rock bridges – overcoming their frictional strength and cohesion (and in some cases tensile strength) if irreversible deformation occurs [*Erismann and Abele*, 2001]. Depending on the persistence of the discontinuities and the spatial movement mode the importance of these resistive forces varies [*Eberhardt et al.*, 2004] and time-dependent processes such as sub-critical fracture growth [*Atkinson*, 1982] may play a decisive role for rockfall release. For transient effects on the resistive strengths in permafrost bedrock, changes in temperature and hydrology are possible explanations. In contrast to dry clefts, frozen cleft infill causes significant cohesion or possibly even short-term adhesion (i.e., tensile strength) that is sensitive to temperature [*Krautblatter*, 2009] while the build-up of a hydrostatic pressure reduces the normal stress and correspondingly reduces the shear strength of clefts. These two mechanisms of strength reduction of clefts in permafrost areas may be responsible for thawing related increase of cleft movements and are discussed in the following.

[39] The tensile strength and cohesion of intact, water saturated rock increases with lower sub-zero temperatures [*Mellor*, 1973]. Furthermore, laboratory experiments show that the shear strength of an ice-filled cleft becomes minimal if the temperature approaches 0°C and (brittle) failure at the rock-ice interface occurs [*Davies et al.*, 2001; *Ladanyi*, 2006; *Guenzel*, 2008]. The transfer of laboratory results to field situations is problematic as the time scales considered in the laboratory are on the order of minutes to hours as compared days to months in the field. As the compensation of stress in ice-filled clefts depends on ductile ice deformation rates [*Guenzel*, 2008; *Ladanyi*, 2006] similar deformation rates as detected in the laboratory would result in unrealistic large deformation in the field ($\gg$cm/y). This means that the effect of pure ice infill cannot stabilize an open cleft under long-term mechanical stress [*Krautblatter*, 2009]. The stabilizing effect must be attributed to the prevention of water pressure build-up at depth [*Gruber and Haeberli*, 2007] or to additional friction by rock-rock contacts due to fracture roughness or debris and clay infill, which both show a dependency on sub-zero temperatures [*Krautblatter*, 2009; *Ladanyi*, 2006].

[40] The enhanced expansion and shearing described above shows similarities with the seasonal pattern of permafrost creep in rock glaciers [*Arenson et al.*, 2002; *Perruchoud and Delaloye*, 2007; *Ikeda et al.*, 2008]. Similarly to the temperature-dependent reduction of the internal friction of a rock-ice mixture in rock glaciers, the warming of cleft-ice or frozen cleft infill may be responsible for enhanced toppling and sliding movements of large blocks in rock slopes. The shearing recorded in summer can be explained by such a reduction of the shear strength in the (steeply dipping) clefts found between individual blocks. Because the thermomechanically induced stress is not constant over time (Hypothesis 1), additional short-term stress is withstood by the ice (ductile deformation). The reduction of shearing movements recorded during winter corresponds to such a mechanism. The sudden change in the shearing regime points to a warming caused by water percolation and related heat release or water pressure build-up. The same is true for the rapid response of the summer expansion at C2 and constant temperatures at 0°C (zero-curtain) which indicate water percolation. In contrast, at C3 a gradual response to the rock warming and the absence of a zero-curtain indicates no water percolation. The clefts at this northern oriented location are influenced by warming due to heat conduction in the rock that may cause changes in the cleft strength. In the case of C2, where we assume a gravity driven instability, the temporal movement during the summer expansion phase does not show a simple correlation with temperature or precipitation once the enhanced opening is triggered. Time-dependent

processes such as sub-critical fracture propagation [*Kemeny*, 2003] or stick-slip shear failure [*Byerlee*, 1970] appear to be involved in these movements. However, their occurrence during the thawing seasons and the clustering of large movements (slips) in the afternoon may indicate that the conditions for these processes are not independent from temperature.

[41] Even though it is unclear if some of these warming-related movements will climax in a significant failure event, common mechanisms with pre-failure deformations are likely. The response to thawing within hours to weeks in the near-surface cleft may be an explanation for the early timing of rockfall in the European Alps in the hot summer of 2003 [*Gruber et al.*, 2004]. At the same time, the strong sensitivity to water percolation could be a reason for no clear correlation between rockfall activity and warm permafrost conditions [*Noetzli et al.*, 2003; *Fischer*, 2010]. In bedrock permafrost, the direct response of rock stability to short-term warming seems to be characteristic of only one type of rockfall release. Alternative mechanisms, such as the accumulation of an irreversible part of cleft expansion (temperature-correlated dilatation regime) or freezing related mechanisms could be relevant in other situations.

6. Conclusions

[42] The interaction of physical processes that govern rockfall hazard from permafrost mountain slopes is poorly understood at present. In this study we have used high-resolution temperature and cleft movement records from the Matterhorn Hörnligrat (Switzerland) to analyze the interaction between the thermal conditions and the relative movements at these large open fractures. The movements observed at 10 clefts show differences in amplitude and response time but commonality in patterns: During most of the year the cleft expansion is negatively correlated to the rock or cleft temperature with an occasionally increased expansion rate in autumn. Conversely opening occurs at two clefts in summer when minimal cleft aperture would be expected according to the described negative correlation. The initiation of this summer opening is synchronized to snowmelt and stops with the first intense freezing in autumn. Significant shearing activity is restricted to this time span as well. The response of both movement types to the thermal conditions at the near-surface is within hours to a few weeks.

[43] Based on the review and discussion of existing explanations for rock and cleft movements we state the following two hypotheses on the physical processes that cause movement of large clefts in permafrost bedrock:

1. Temperature-correlated cleft expansion mainly originates from thermomechanical forcing and from cryogenic processes within the cleft driving increased autumn dilatation.

2. Shearing and exceptional expansion that occur during the melting season are explained by a (shear-) strength reduction of rock–rock contacts, the rock–ice interface or ice-cemented infill within clefts. This is caused by conductive warming and meltwater percolation with related hydro-static pressure build-up or latent heat release.

[44] In view of rock slope failure in permafrost the processes in Hypothesis 1 are relevant as disposition factors. The accumulation of irreversible movements modifies the geometrical setting of large blocks and can slowly bring them to a critical state. Clefts influenced by such large movements would not be permanently ice-sealed and thus may be more sensitive to water percolation. Ice segregation is an unlikely explanation for the recorded movements (Subsection 5.2) however it could play an important role in fracture propagation and the development of planes of weakness in frozen rock [*Hallet et al.*, 1991]. This effect is expected to be very inert in fine porous hard rock [*Matsuoka*, 2001b] with timescales in the order of decades to centuries and is therefore not measurable with our current setup.

[45] Hypothesis 2 concerns mechanisms that can modify slope stability rapidly. It is likely that the postulated decrease in the mechanical strength of clefts is involved in the release of warming-related rockfall from permafrost slopes. Where the stability of rock masses is critical due to the geological, structural and topographic settings such short-term variations of strength parameters can trigger failures. The fast response of both the movements derived from the time series data presented here and rockfall activity observed [*Gruber et al.*, 2004] points to the high importance of the hydrothermal processes. Even though different mechanisms are assumed (see Section 5.3) to link water percolation and stability their sensitivity to snowmelt and liquid precipitation is similar. The investigation of the evolution and movement mode of such warming related rock movements with respect to the thermal and hydrological conditions at the shearing planes may be a key for the understanding of summer rockfall from permafrost areas.

Notations

x	expansion of the cleft perpendicular crack meter [mm]
Δx	cleft expansion minus to initial value (x_0): $\Delta x = x\text{-}x_0$ [mm]
Δy	cleft shearing in dip direction parallel to cleft surface [mm]
dx/dt	expansion rate [m/s]
dx/dT	thermal cleft expansion gradient [mm/°C]
dT/dt	temporal derivative of temperature (warming rate) [°C/s]

[46] **Acknowledgments.** We would like to thank the PermaSense team, R. Lim, M. Yücel, I. Talzi, T. Gsell, M. Keller, L. Thiele and C. Tschudin who made this challenging measurement possible. Thanks to P. Pogliotti and L. Fischer for the support with the geological interpretation in the field and V. Gischig and J. Moore for the discussions and their advice. The research presented within the project PermaSense was funded by the Swiss Federal Office for the Environment (FOEN) and the National Competence Center on Mobile Information and Communication Systems NCCR MICS of the Swiss National Science Foundation (SNSF).

References

Akagawa, S., and M. Fukuda (1991), Frost heave mechanism in welded tuff, *Permafrost Periglacial Processes*, *2*(4), 301–309, doi:10.1002/ppp.3430020405.

Amitrano, D., M. Arattano, M. Chiarle, G. Mortara, C. Occhiena, M. Pirulli, and C. Scavia (2010), Microseismic activity analysis for the study of the rupture mechanisms in unstable rock masses, *Nat. Hazards Earth Syst. Sci.*, *10*, 831–841.

Arenson, L., M. Hoelzle, and S. Springman (2002), Borehole deformation measurements and internal structure of some rock glaciers in Switzerland, *Permafrost Periglacial Processes*, *13*(2), 117–135, doi:10.1002/ppp.414.

Atkinson, B. K. (1982), Subcritical crack propagation in rocks: Theory, experimental results and applications, *J. Struct. Geol.*, *4*(1), 41–56, doi:10.1016/0191-8141(82)90005-0.

Beutel, J., et al. (2009), PermaDAQ: A scientific instrument for precision sensing and data recovery in environmental extremes, paper presented at 2009 International Conference on Information Processing in Sensor Networks, IEEE Comp. Soc., San Francisco, Calif.

Braathen, A., L. H. Blikra, S. S. Berg, and F. Karlsen (2004), Rock-slope failures of Norway, type, geometry deformation mechanisms and stability, *Norw. J. Geol.*, *84*(1), 67–88.

Byerlee, J. D. (1970), The mechanics of stick-slip, *Tectonophysics*, *9*(5), 475–486, doi:10.1016/0040-1951(70)90059-4.

Coussy, O. (2005), Poromechanics of freezing materials, *J. Mech. Phys. Solids*, *53*(8), 1689–1718, doi:10.1016/j.jmps.2005.04.001.

Cruden, D. M. (2003), The shapes of cold, high mountains in sedimentary rocks, *Geomorphology*, *55*(1–4), 249–261, doi:10.1016/S0169-555X(03)00143-0.

Davies, M. C. R., O. Hamza, and C. Harris (2001), The effect of rise in mean annual temperature on the stability of rock slopes containing ice-filled discontinuities, *Permafrost Periglacial Processes*, *12*(1), 137–144, doi:10.1002/ppp.378.

Eberhardt, E., D. Stead, and J. S. Coggan (2004), Numerical analysis of initiation and progressive failure in natural rock slopes–the 1991 Randa rockslide, *Int. J. Rock Mech. Min. Sci.*, *41*(1), 69–87, doi:10.1016/S1365-1609(03)00076-5.

Erismann, T. H., and G. Abele (2001), *Dynamics of Rockslides and Rockfalls*, Springer, New York.

Fischer, L. (2010), Slope instabilities on perennially frozen and glacierized rock walls: Multi-scale observations, analyses and modelling, PhD thesis, Univ. of Zurich, Zurich, Switzerland.

Fischer, L., F. Amann, J. R. Moore, and C. Huggel (2010), Assessment of periglacial slope stability for the 1988 Tschierva rock avalanche (Piz Morteratsch, Switzerland), *Eng. Geol. Amsterdam*, *116*(1–2), 32–43, doi:10.1016/j.enggeo.2010.07.005.

Fukuda, M. (1983), The pore water pressure profile in porous rocks during freezing, in *Permafrost: Fourth International Conference, Proceedings*, pp. 322–327, Natl. Acad. Press, Washington, D. C.

Gischig, V. S., J. R. Moore, K. F. Evans, F. Amann, and S. Loew (2011a), Thermomechanical forcing of deep rock slope deformation: 1. Conceptual study of a simplified slope, *J. Geophys. Res.*, *116*, F04010, doi:10.1029/2011JF002006.

Gischig, V. S., J. R. Moore, K. F. Evans, F. Amann, and S. Loew (2011b), Thermomechanical forcing of deep rock slope deformation: 2. The Randa rock slope instability, *J. Geophys. Res.*, *116*, F04011, doi:10.1029/2011JF002007.

Gruber, S., and W. Haeberli (2007), Permafrost in steep bedrock slopes and its temperature-related destabilization following climate change, *J. Geophys. Res.*, *112*, F02S18, doi:10.1029/2006JF000547.

Gruber, S., M. Hoelzle, and W. Haeberli (2004), Permafrost thaw and destabilization of Alpine rock walls in the hot summer of 2003, *Geophys. Res. Lett.*, *31*, L13504, doi:10.1029/2004GL020051.

Guenzel, F. (2008), Shear strength of ice-filled rock joints, in *Proceedings of the 9th International Conference on Permafrost*, pp. 581–586, Univ. of Alaska, Fairbanks, Alaska.

Gunzburger, Y., V. Merrien-Soukatchoff, and Y. Guglielmi (2005), Influence of daily surface temperature fluctuations on rock slope stability: Case study of the Rochers de Valabres slope (France), *Int. J. Rock Mech. Min. Sci.*, *42*(3), 331–349, doi:10.1016/j.ijrmms.2004.11.003.

Haeberli, W., M. Wegmann, and D. Vonder Muehll (1997), Slope stability problems related to glacier shrinkage and permafrost degradation in the Alps, *Eclogae Geol. Helv.*, *90*, 407–414.

Hallet, B., J. S. Walder, and C. W. Stubbs (1991), Weathering by segregation ice growth in microcracks at sustained sub-zero temperatures: Verification from an experimental study using acoustic emissions, *Permafrost Periglacial Processes*, *2*(4), 283–300, doi:10.1002/ppp.3430020404.

Hasler, A., I. Talzi, J. Beutel, C. Tschudin, and S. Gruber (2008), Wireless sensor networks in permafrost research: Concept, requirements, implementation, and challenges, in *Proceedings of the 9th International Conference on Permafrost*, pp. 669–674, Univ. of Alaska, Fairbanks, Alaska.

Hasler, A., S. Gruber, and W. Haeberli (2011a), Temperature variability and thermal offset in steep alpine rock and ice faces, *Cryosphere*, *5*, 977–988, doi:10.5194/tc-5-977-2011.

Hasler, A., S. Gruber, M. Font, and A. Dubois (2011b), Advective heat transport in frozen rock clefts: Conceptual model, laboratory experiments and numerical simulation, *Permafrost Periglacial Processes*, *22*(4), 378–389, doi:10.1002/ppp.737.

Hiebl, J., et al. (2009), A high-resolution 1961–1990 monthly temperature climatology for the greater Alpine region, *Meteorol. Z.*, *18*(5), 507–530, doi:10.1127/0941-2948/2009/0403.

Ikeda, A., N. Matsuoka, and A. Kääb (2008), Fast deformation of perennially frozen debris in a warm rock-glacier in the Swiss Alps: An effect of liquid water, *J. Geophys. Res.*, *113*, F01021, doi:10.1029/2007JF000859.

Kemeny, J. (2003), The time-dependent reduction of sliding cohesion due to rock bridges along discontinuities: A fracture mechanics approach, *Rock Mech. Rock Eng.*, *36*(1), 27–38, doi:10.1007/s00603-002-0032-2.

Krautblatter, M. (2009), Detection and quantification of permafrost change in alpine rock walls and implications for rock instability, PhD thesis, Rheinischen Friedrich-Wilhelms-Univ. Bonn, Bonn, Germany.

Lachenbruch, A. H. (1962), *Mechanics of Thermal Contraction Cracks and Ice-Wedge Polygons in Permafrost*, Geol. Soc. of Am., New York.

Ladanyi, B. (2006), Creep of frozen slopes and ice-filled rock joints under temperature variation, *Can. J. Civ. Eng.*, *33*(6), 719–725, doi:10.1139/l05-112.

Matsuoka, N. (2001a), Direct observation of frost wedging in alpine bedrock, *Earth Surf. Processes Landforms*, *26*(6), 601–614, doi:10.1002/esp.208.

Matsuoka, N. (2001b), Microgelivation versus macrogelivation: Towards bridging the gap between laboratory and field frost weathering, *Permafrost Periglacial Processes*, *12*(3), 299–313, doi:10.1002/ppp.393.

Matsuoka, N. (2008), Frost weathering and rockwall erosion in the southeastern Swiss Alps: Long-term (1994–2006) observations, *Geomorphology*, *99*(1–4), 353–368, doi:10.1016/j.geomorph.2007.11.013.

Matsuoka, N., and J. Murton (2008), Frost weathering: Recent advances and future directions, *Permafrost Periglacial Processes*, *19*(2), 195–210, doi:10.1002/ppp.620.

Mellor, M. (1973), Mechanical properties of rocks at low temperatures, in *Permafrost: Second International Conference*, pp. 334–344, Natl. Acad. of Sci., Washington, D. C.

Mufundirwa, A., Y. Fujii, N. Kodama, and J. Kodama (2011), Analysis of natural rock slope deformations under temperature variation: A case from a cool temperate region in Japan, *Cold Reg. Sci. Technol.*, *65*(3), 488–500, doi:10.1016/j.coldregions.2010.11.003.

Murton, J. B., J. P. Coutard, J. P. Lautridou, J. C. Ozouf, D. A. Robinson, and R. B. G. Williams (2001), Physical modelling of bedrock brecciation by ice segregation in permafrost, *Permafrost Periglacial Processes*, *12*(3), 255–266, doi:10.1002/ppp.390.

Murton, J. B., R. Peterson, and J. C. Ozouf (2006), Bedrock fracture by ice segregation in cold regions, *Science*, *314*(5802), 1127–1129, doi:10.1126/science.1132127.

Noetzli, J., M. Hoelzle, and W. Haeberli (2003), Mountain permafrost and recent Alpine rock-fall events: A GIS-based approach to determine critical factors, in *Permafrost: Proceedings of 8th International Conference on Permafrost*, pp. 827–832, A.A. Balkema Publ., Exton, Pa.

Noetzli, J., S. Gruber, T. Kohl, N. Salzmann, and W. Haeberli (2007), Three-dimensional distribution and evolution of permafrost temperatures in idealized high-mountain topography, *J. Geophys. Res.*, *112*, F02S13, doi:10.1029/2006JF000545.

Nordvik, T., L. H. Blikra, E. Nyrnes, and M. H. Derron (2010), Statistical analysis of seasonal displacements at the Nordnes rockslide, northern Norway, *Eng. Geol. Amsterdam*, *114*, 228–237, doi:10.1016/j.enggeo.2010.04.019.

Perruchoud, E., and R. Delaloye (2007), Short-term changes in surface velocities on the Becs-de-Bosson rock glacier (western Swiss Alps), in *Proceedings of the 8th International Symposium on High Mountain Remote Sensing Cartography*, *Grazen Schr. der Geogr. und Raumforschung*, vol. 41, pp. 14–15, Inst. Geogr. Reg. Sci., Graz, Austria.

Pirulli, M. (2009), The Thurwieser rock avalanche (Italian Alps): Description and dynamic analysis, *Eng. Geol. Amsterdam*, *109*(1–2), 80–92, doi:10.1016/j.enggeo.2008.10.007.

Pleuger, J., S. Roller, J. M. Walter, E. Jansen, and N. Froitzheim (2007), Structural evolution of the contact between two Penninic nappes (Zermatt-Saas zone and Combin zone, Western Alps) and implications for the exhumation mechanism and palaeogeography, *Int. J. Earth Sci.*, *96*, 229–252, doi:10.1007/s00531-006-0106-6.

Ravanel, L., and P. Deline (2010), Climate influence on rockfalls in high-Alpine steep rockwalls: The north side of the Aiguilles de Chamonix (Mont Blanc massif) since the end of the Little Ice Age, *Holocene*, *21*, 357–365, doi:10.1177/0959683610374887.

Savage, W. Z., and D. J. Varnes (1987), Mechanics of gravitational spreading of steep-sided ridges (sackung), *Bull. Eng. Geol. Environ.*, *35*(1), 31–36, doi:10.1007/BF02590474.

Talzi, I., A. Hasler, S. Gruber, and C. Tschudin (2007), PermaSense: Investigating permafrost with a WSN in the Swiss Alps, paper presented at 4th Workshop on Embedded Networked Sensors, Assoc. Comput. Mach., Cork, Ireland.

Watson, A. D., D. P. Moore, and T. W. Stewart (2004), Temperature influence on rock slope movements at Checkerboard Creek, in *Landslides:*

Evaluation and Stabilization, Proceedings of the 9th International Symposium on Landslides, pp. 1293–1298, A. A. Balkema Publ., Exton, Pa.

Wegmann, M. (1998), *Frostdynamik in hochalpinen Felswänden am Beispiel der Region Jungfraujoch-Aletsch*, *Mitt. der Vers. für Wasserbau, Hydrol. und Glaziol. der ETH Zürich*, vol. 161, ETH Zurich, Zurich, Switzerland.

Wegmann, M., and G. Gudmundsson (1999), Thermally induced temporal strain variations in rock walls observed at subzero temperatures, in *Advances in Cold-Region Thermal Engineering and Sciences*, pp. 511–518, Springer, New York.

J. Beutel, Computer Engineering and Networks Laboratory, ETH Zurich, Gloriastr. 35, CH-8092 Zurich, Switzerland. (janbeutel@ethz.ch)

S. Gruber and A. Hasler, Glaciology, Geomorphodynamics and Geochronology, Department of Geography, University of Zurich, Winterthurerstr. 190, CH-8057 Zurich, Switzerland. (stephan.gruber@geo.uzh.ch; andreas.hasler@geo.uzh.ch)